INL/CON-15-36535
PREPRINT

Development of a Verification Benchmark Suite for the ATR Reactor Physics Upgrade

Physics of Reactors Conference (PHYSOR 2016)

B. Ganapol
(University of Arizona)

D. Nigg
(Idaho National Laboratory)

May 2016

The INL is a
U.S. Department of Energy
National Laboratory
operated by
Battelle Energy Alliance

DEVELOPMENT OF A VERIFICATION BENCHMARK SUITE FOR THE ATR REACTOR PHYSICS UPGRADE

B. Ganapol
Department of Aerospace and Mechanical Engineering
University of Arizona, Tucson, AZ, USA
Ganapol@cowboy.ame.arizona.edu

D. Nigg
Nuclear Systems Design and Analysis Division
Idaho National Laboratory, Idaho Falls, Idaho, USA
DWN@INL.Gov

ABSTRACT

A result of a numerical algorithm is only as good as the effort made towards its verification. Comprehensive computer codes, especially for application to nuclear reactors, require in-depth assessment of the numerical methods used and their computational implementation. This presentation describes a suite of semi-analytical benchmarks for the ATR Reactor Physics Upgrade as part of the ATR Life Extension Project (LEP). Several neutron transport codes including deterministic codes HELIOS, NEWT and probabilistic codes MCNP6, SERPENT and MC21 are upgrade candidates. To properly evaluate performance capabilities, code verification is an essential element. A credible verification program requires education to guide proper application, training in proper input preparation and output expectation and verification to instill confidence in the coded numerical procedures. The subset of the benchmark suite to be described is primarily of the 1D transport variety however, a 2D case is included, with the intent to provide unquestionably high order accurate semi-analytical numerical benchmark solutions. In this presentation, we base the analytical solutions presented on analytical Fourier series representations. There is also a corresponding effort based on discrete ordinates, which will not be considered here.

Key Words: **Fourier series, Neutron transport, Benchmark, Wynn-epsilon acceleration, Infinite lattice**

1. INTRODUCTION

Regardless of application, every neutron transport code, new or legacy, requires verification. This is

particularly true for the ATR Reactor Physics Upgrade Project [1], which is part of the ATR Life Extension Project (LEP) recently concluded at INL. The project's objective is to provide the ATR facility with a robust modern-day reactor physics capability through a suite of current, well-established, reactor physics codes to include both deterministic and probabilistic options. These codes consist of the lead 2D transport criticality code HELIOS, followed by candidate deterministic codes NEWT and Monte Carlo codes MCNP6, SERPENT and MC21. A considerable effort has gone into the development of these codes at four national laboratories and at a private company. While they are the product of some of today's top computational transport methods developers; nevertheless, the codes are not, and, arguably will never be, entirely error free. For this reason, a program of vigilant verification, even for widely used routine legacy codes, must be an ongoing process that is fully supported by the institutions responsible for their development.

1.1. Scope of Benchmark Suite

Table 1 identifies a roadmap of the benchmarks considered using the two fundamental computational strategies. A "√" indicates what has been established to date as the minimal benchmark. Note that the development progresses in stages leading to more comprehensive benchmarks with each including the early stage development. The ultimate goal was to fill in all categories; however, as the table shows, primarily only one-dimensional benchmarks were completed. What we presented is, for the most part, innovation in solving and evaluating the solutions of the transport equation. While the primary effort was to reach the LEP milestone and provide reliable HELIOS benchmarks, the solutions and methods presented are also of general academic interest by themselves.

Table 1. Benchmark Suite Roadmap

Benchmark	**1*D***	**2*D***	***One- group***	***Multigroup***
Single region with source	√	√	√	√
Two region with source	√		√	√
Many region with source	√		√	√
Two region criticality	√		√	√
Many region criticality	√		√	√

2. 1D CELL BENCHMARKS

We first consider a semi-analytical benchmark for the 1D cell generated by a discrete Fourier series (FS) similar to that recently published [2]. The motivation for this approach, as initially suggested by

MMR Williams in Ref. 2, is consideration of a single cell conveniently simplifies to one of infinite extent since the cell is replicated as a consequence of the naturally imposed zero current at cell interfaces. This greatly simplifies the transport solution since boundary conditions are avoided.

We begin the theory development with straightforward transport in a 1D slab in the multigroup approximation. Figure 1 shows the configuration to be investigated for a simple symmetric cell of two

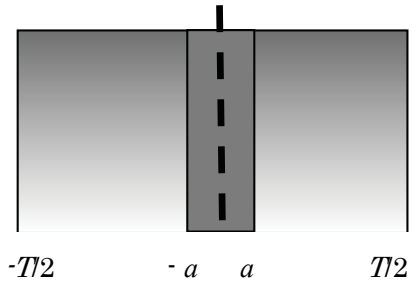

Fig. 1. Uniform cell with source.

regions. The cell is a unit of a 1D infinite reactor lattice and is commonly constructed to represent cell average behavior. For anisotropic scattering, the 1D multigroup neutron transport equation reads as

$$\left[\mu \boldsymbol{I}\frac{\partial}{\partial x}+\boldsymbol{\Sigma}\right]\boldsymbol{\phi}(x,\mu)=\frac{1}{2}\sum_{l=0}^{L}(2l+1)P_l(\mu)\boldsymbol{\Sigma}_{sl}(x)\boldsymbol{\phi}_l(x)+\boldsymbol{S}(x,\mu), \tag{1a}$$

where the following definitions hold:

$$\boldsymbol{\phi}(x,\mu)\equiv\left[\phi_1(x,\mu)\quad\phi_2(x,\mu)\quad\ldots.\quad\phi_G(x,\mu)\right]^T$$
$$\phi_g(x,\mu)\equiv\int_{\Delta E_g}dE\phi(x,\mu,E)$$
$$\boldsymbol{\Sigma}_f(x)\equiv\left[\Sigma_{f1}(x)\quad\Sigma_{f2}(x)\quad\ldots.\quad\Sigma_{fG}(x)\right]^T$$
$$\boldsymbol{\chi}\equiv\left[\chi_1\quad\chi_2\quad\ldots.\quad\chi_G\right]^T \tag{1b,c,d,e,f,g}$$
$$\boldsymbol{\phi}_l(x)=\int_{-1}^{1}d\mu P_l(\mu)\boldsymbol{\phi}(x,\mu)$$
$$\boldsymbol{\Sigma}(x)\equiv diag\left\{\Sigma_g(x);\ g=1,2,...,G\right\}$$
$$\boldsymbol{\Sigma}_{sl}(x)\equiv\left\{\boldsymbol{\Sigma}_{slg,g'}(x);\ g,g'=1,2,...,G\right\}$$

For analytical tractability, we must assume

$$\boldsymbol{\Sigma}(x)\equiv\xi(x)diag\left\{\overline{\Sigma}_g\right\}=\xi(x)\overline{\boldsymbol{\Sigma}}, \tag{2}$$

where $\overline{\boldsymbol{\Sigma}}$ is constant across the cell giving the replacements

$$x \to \int_0^x dx' \xi(x'),\ \boldsymbol{\Sigma}_{sl}(x) \to \boldsymbol{\Sigma}_{sl}(x)/\xi(x),\ \boldsymbol{\Sigma}(x) \to I,\ \boldsymbol{S}(x,\mu) \to \boldsymbol{S}(x,\mu)/\xi(x)$$

Assuming isotropic scattering, the replicating nature of the cells enables a discrete Fourier series solution representation of the flux and source group vectors and the group cross section matrices of the form,

$$\sum_{n=0}^{\infty}\left[\delta_{k,n}\boldsymbol{I} - \boldsymbol{L}_{00}(\alpha_k)\boldsymbol{\Sigma}^{+}_{s0,k,n}\right]\boldsymbol{\phi}_{n,0} = \boldsymbol{L}_{00}(\alpha_k)\boldsymbol{S}_{k,0},\ k = 0,1,..., \tag{3a}$$

where

$$\boldsymbol{\Sigma}^{+}_{s0,k,n} = \begin{cases} \boldsymbol{\Sigma}_{s0,k}, & n=0 \\ \boldsymbol{\Sigma}_{s0,k-n} + \boldsymbol{\Sigma}_{s0,k+n}, & n \geq 1 \end{cases}$$

$$\alpha_n \equiv \frac{2\pi n}{T} \tag{3b,c}$$

$$\boldsymbol{L}_{00}(\alpha_k) = \boldsymbol{\Sigma}^{-1} diag\left\{\frac{tan(\alpha_k/\Sigma_{gg})}{\alpha_k/\Sigma_{gg}}\right\} \equiv \boldsymbol{T}(\alpha_k\boldsymbol{\Sigma}^{-1});$$

and $\boldsymbol{S}_{k,0}$ is the isotropic source Fourier component. Once we find the zeroth moment $\boldsymbol{\phi}_{n,0}$, the scalar flux becomes

$$\boldsymbol{\phi}_0(x) = \lim_{N\to\infty}\sum_{n=0}^{N}\left[2-\delta_{n,0}\right]\boldsymbol{\phi}_{n,0}\cos(\alpha_n x) \tag{4}$$

We now consider several cases.

2.1. One- Group/Single Homogeneous Cell with Source/No Fission

Our first numerical demonstration will be for a uniform slab in the one-group approximation with a symmetric source embedded in region [$-T_s/2$, $T_s/2$]. While this may seem an overly simplified case, it actually is not. Since we are considering a homogeneous medium, the nuclear density is $\xi(x)$ and naturally cancels out. Thus, the density of the single material, which itself could be a mixture, can vary across the slab as one wishes.

2.1.1. Implementation and Verification

For this case, the source is uniform in region $|x| \leq T_s/2$ and the flux Fourier moments become

$$\phi_{n,0} = \frac{T(\alpha_n)}{1 - c_s T(\alpha_n)} S(\alpha_n) \tag{5a}$$

with

$$S(\alpha_n) \equiv S_{n,0} = \frac{1}{T}\left[\frac{\sin(\alpha_n T_s / 2)}{\alpha_n T_s / 2}\right] Q_0 \tag{5bc}$$

$$T(\alpha_n) \equiv \frac{\tan^{-1}(\alpha_n)}{\alpha_n}$$

giving the scalar flux

$$\phi_0(x) = \frac{1}{T}\left\{\frac{1}{1 - c_s} + 2\sum_{n=1}^{\infty}\left[\frac{T(\alpha_n)}{1 - c_s T(\alpha_n)}\right]\left[\frac{\sin(\alpha_n T_s / 2)}{\alpha_n T_s / 2}\right]\cos(\alpha_n x)\right\}. \tag{6}$$

The most difficult task in implementation of the scalar flux is the evaluation of the Fourier series. Because of its slow convergence and oscillatory nature, a converged numerical series requires special treatment. In particular, subtraction of the series form of the uncollided contribution and addition of an analytical uncollided form greatly improves convergence. In addition, acceleration of the partial sums by Wynn-epsilon acceleration [3] is enabling. Several internal checks on the precision of series of Eq(3) confirm its adequacy to give highly precise results to at least 6-places.

2.1.2. Demonstration

Figures 1a,b are provided to demonstrate that the 1-Group/1D Cell single material benchmark gives intuitive variation of source single scatter albedo over 8 and 32 cell lattices. The variation is for the scattering secondaries over the cells for a single cell and source thickness of 5*mfp* and 1*mfp* respectively. Note that the flux was determined in a single calculation using cell periodicity and not simply reproduced from a single cell.

2.2. Multigroup/Single Region with Symmetric Source

We now turn to an example of a multigroup version of neutron transport in a homogeneous cell however without fission neutrons-- but still assuming isotropic scattering and a spatially uniform source in $|x| \le T_s / 2$ for all groups. One eliminates fission neutrons by setting the fission spectrum to zero. For this case, since the scattering cross section remains constant across the cell for the multigroup approximation, we find

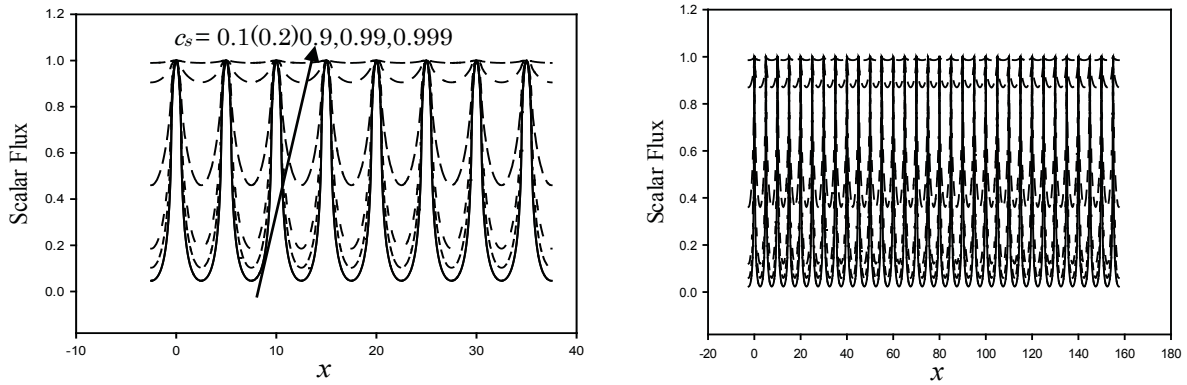

Fig. 1a,b. Variation of the number of secondaries over 8 cell and 32 cells.

$$\boldsymbol{\phi}_{n,0} = \left[\boldsymbol{\Sigma} - \boldsymbol{T}\left(\alpha_n \boldsymbol{\Sigma}^{-1}\right)\boldsymbol{\Sigma}_{s0,0}\right]^{-1} \boldsymbol{T}\left(\alpha_n \boldsymbol{\Sigma}^{-1}\right)\boldsymbol{S}\left(\alpha_n\right),\ n = 0,1,\ldots\ . \tag{7a}$$

with

$$\boldsymbol{\Sigma}^{+}_{s0,nk} = \boldsymbol{\Sigma}_{s0,0} \begin{cases} \delta_{n,0}, n{=}0 \\ \delta_{n,k}, n \geq 1 \end{cases} \tag{7b}$$

$$\boldsymbol{S}\left(\alpha_n\right) \equiv \boldsymbol{S}_{n,0} = \frac{1}{T}\left[\frac{\sin\left(\alpha_n T_s / 2\right)}{\alpha_n T_s / 2}\right]\boldsymbol{Q},$$

where $\boldsymbol{Q}$ is the source energy distribution. The final solution comes from the vector form of Eq(4) once the vector Fourier components are found from Eq(7a).

2.2.1. Implementation and Verification

We follow the same numerical procedure as for the one-group case with a slight modification. All group wise components $\phi_{0g}(x;N)$ in the partial sums are interrogated for convergence either as is or by *W-e* acceleration. Convergence occurs when all component partial sums in the group vector have converged to the desired relative error. In addition, the Fourier series is over converged by one or two orders to achieve additional precision, which simply amounts to decreasing the relative error by the corresponding orders of magnitude. In experimenting with the multigroup numerical evaluation, it became obvious that to maintain accuracy to at least 6 or 7 places, separate uncollided contributions are required as in the one group case.

To verify the implementation of this algorithm, we first confirm against the one-group benchmark. In particular, the test case is $c_s = 0.9$, $T = 5$, $T_s = 0.25$ with $\boldsymbol{Q}$ a vector of all ones. As observed in Table 2, for a requested error of 10^{-10}, with this procedure, we find solid 8-place agreement with the one-

group energy flux. For the usual error request of 10^{-6}, we see compliance to six places for all except two entries.

2.2.2. Demonstration

The following examples demonstrate and intuitively test the multigroup calculation directly. For the cases to follow, we capture data from the BNL/ENDF website [4] over the spectral range 20*Mev* down to 0.1*ev*, nominally assuming a homogeneous mixture of 10% ^{235}U and 90% ^{12}C and elastic scattering exclusively. The group structure is uniform in lethargy and the source is in a thin first group of width $0.001 \times E_0$.

Table 2. One-group comparison with the multigroup algorithm ($c_s = 0.9$, $T = 5$ and $T_s = 0.25$)

x	10^{-6}	10^{-8}	10^{-10}	*One Gp*
0.000000E+00	3.897052240E+00	3.897052411E+00	3.897052411E+00	3.897052411E+00
5.000000E-02	3.850045205E+00	3.850044052E+00	3.850044050E+00	3.850044051E+00
1.000000E-01	3.689570605E+00	3.689569373E+00	3.689569313E+00	3.689569309E+00
1.250000E-01	3.513858485E+00	3.513858486E+00	3.513858486E+00	3.513858486E+00
6.000000E-01	2.337548460E+00	2.337548482E+00	2.337548483E+00	2.337548483E+00
1.550000E+00	1.606522912E+00	1.606522910E+00	1.606522910E+00	1.606522910E+00
2.500000E+00	1.409497665E+00	1.409497707E+00	1.409497707E+00	1.409497707E+00

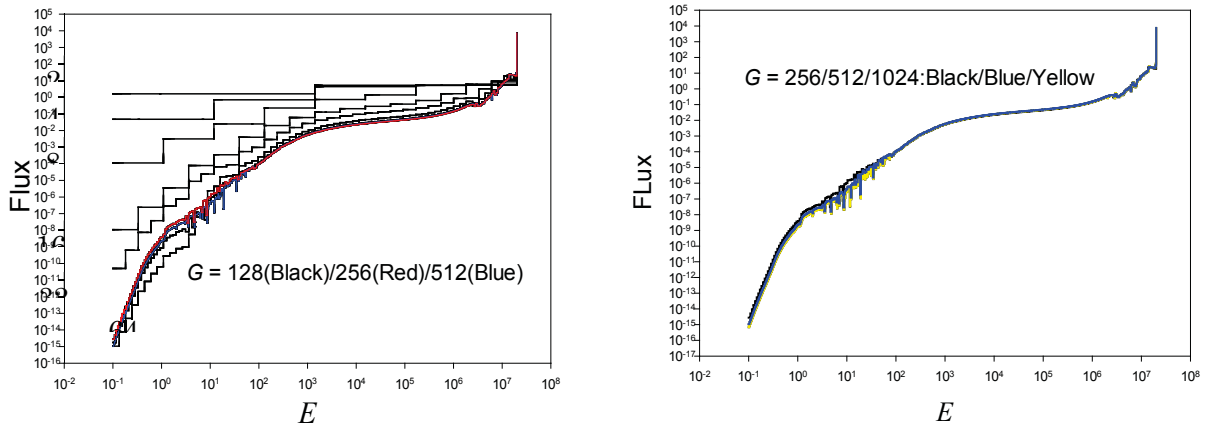

Fig.2. (a) Visual spectral convergence: *G*=128(black)/256(red)/512(blue)
(b) *G* = 256 in Black/G=512 in blue/1024 in Yellow.

Figures 2a,b show convergence in group structure up to and including 1024 groups, further confirming convergence and demonstrating that this benchmark is sufficiently robust to be of the fine group

variety. Note that the ability of the fuel to effectively absorb neutrons especially at low energies, accounts for the uncharacteristically small flux.

3. 2D CELL BENCHMARKS

3.1. 2D Theory for the Homogeneous Cell

Next, we examine the 2D square homogeneous cell with guidance from our 1D investigations. For the 2D benchmark, we consider only the single region with a fixed circular source region of radius a or square source region of side T_s primarily in the one-group and briefly in the multigroup approximations. 2D transport benchmarks are noticeably more difficult than 1D transport benchmarks.

Considering only isotropic scattering and source emission in a homogeneous medium, the appropriate 2D multigroup transport equation in Cartesian coordinates is

$$\left[\Omega\bullet\nabla \boldsymbol{I} + \boldsymbol{\Sigma}\right]\boldsymbol{\phi}(x,y,\Omega) = \frac{1}{4\pi}\boldsymbol{\Sigma}_{s0}\boldsymbol{\phi}_0(x,y) + \frac{1}{4\pi}\boldsymbol{S}(x,y)\cdot \tag{8}$$

The initial 2D configuration to consider is for an infinite lattice of square cells with a central cylindrical source as shown

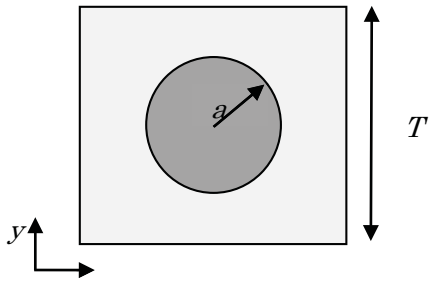

Fig. 3. 2D Cell with a fixed source of radius a.

In the following theoretical description, the reader is referred to reference [2] for more details.

The natural extension of 1D to 2D is

$$\boldsymbol{\phi}(x,y,\Omega) = \sum_{m,n=-\infty}^{\infty} \boldsymbol{\phi}_{mn}(\Omega) e^{i\alpha_n x + i\alpha_m y}, \tag{9a}$$

which when introduced into Eq(1) gives

$$\left[\boldsymbol{\Sigma} + i\Omega_{mn}\boldsymbol{I}\right]\boldsymbol{\phi}(x,y,\Omega) = \frac{1}{4\pi}\boldsymbol{\Sigma}_{s0}\boldsymbol{\phi}_0(x,y) + \frac{1}{4\pi}\boldsymbol{S}(x,y), \tag{9b}$$

where $\Omega \equiv \Omega(\mu,\psi)$ and

$$\Omega_{mn} \equiv \sqrt{1-\mu^2}\left(\alpha_n \cos\psi + \alpha_m \sin\psi\right). \tag{9c}$$

Then, solving for $\boldsymbol{\phi}(x,y,\Omega)$ and integrating over all directions gives the following Fourier series coefficients for the scalar flux [2]:

$$\boldsymbol{\phi}_{0,mn} = \left[\boldsymbol{I} - \boldsymbol{T}\left(\sqrt{n^2+m^2}\right)\boldsymbol{\Sigma}_{s0}\right]^{-1} \boldsymbol{T}\left(\sqrt{n^2+m^2}\right)\boldsymbol{S}\left(\sqrt{n^2+m^2}\right);\ m,n = 1,2,... \tag{10a}$$

with

$$\boldsymbol{T}\left(\sqrt{\alpha_n^2+\alpha_m^2}\right) \equiv diag\left\{\frac{\tan\left(\sqrt{\alpha_n^2+\alpha_m^2}\,/\,\Sigma_{gg}\right)}{\sqrt{\alpha_n^2+\alpha_m^2}\,/\,\Sigma_{gg}}\right\}. \tag{10b}$$

For the circular source region of radius *a* represented by a similar expansion to the flux, we find the following expansion coefficients:

$$\boldsymbol{S}_{nm} = \begin{bmatrix} \dfrac{\pi a^2}{T^2}, & n=m=0 \\ \dfrac{a}{T\sqrt{n^2+m^2}} J_1\left(\dfrac{2\pi a}{T}\sqrt{n^2+m^2}\right), & otherwise \end{bmatrix} \boldsymbol{Q}_0. \tag{11}$$

Note that finding an analytical representation for the source expansion coefficient enables this benchmark to be of relatively high quality.

Finally, from Eq(4a) and noting symmetry for $m,n \geq 0$

$\boldsymbol{\phi}_{0,mn} = \boldsymbol{\phi}_{0,nm}$

$\boldsymbol{\phi}_{0,-m,n} = \boldsymbol{\phi}_{0,m,-n}$,

the 2D flux is

$$\phi_0(x,y) = \phi_{0,00} + 2\sum_{n=1}^{\infty}\phi_{0,n0}\left[\cos(\alpha_n x)+\cos(\alpha_n y)\right] + \\ + 4\sum_{m,n=1}^{\infty}\phi_{0,mn}\cos(\alpha_n x)\cos(\alpha_m y). \tag{12a}$$

The numerical evaluation proceeds by telescoping the inner sum of the second term and re-indexing to give on truncation of all sums to N,

$$\phi_0(x,y;N) = \phi_{0,00} + 2\sum_{n=1}^{N}\phi_{0,n0}\left[\cos(\alpha_n x)+\cos(\alpha_m y)\right] + \\ + 4\sum_{n=1}^{N}\sum_{l=1}^{n-1}\phi_{0,l,n-l}\cos(\alpha_l x)\cos(\alpha_{n-l} y), \tag{12b}$$

where the series coefficients come from Eq(10a).

3.2. 2D One-group Homogeneous Medium

For the one-group case, all vectors become scalars giving

$$\phi_{0,mn} = \frac{T\left(\sqrt{n^2+m^2}\right)}{\left[I - T\left(\sqrt{n^2+m^2}\right)c\right]}S_{mn}; m,n = 1,2,... \tag{13a}$$

with $c \equiv \Sigma_s / \Sigma$ and

$$T\left(\sqrt{\alpha_n^2+\alpha_m^2}\right) \equiv \frac{\tan\left(\sqrt{\alpha_n^2+\alpha_m^2}\right)}{\sqrt{\alpha_n^2+\alpha_m^2}}. \tag{13b}$$

Finally, $Q_0 = 1$ and the expression to evaluate for the scalar flux is

$$\phi_0(x,y;N) = \phi_{0,00} + 2\sum_{n=1}^{N}\phi_{0,n0}\left[\cos(\alpha_n x)+\cos(\alpha_m y)\right] + \\ + 4\sum_{n=1}^{N}\sum_{l=1}^{n-1}\phi_{0,l,n-l}\cos(\alpha_l x)\cos(\alpha_{n-l} y). \tag{14}$$

Numerical implementation follows that of the previous benchmarks, where a *W-e* acceleration is applied to the Fourier series truncated at *N*. An additive stride of 2 produces the sequence to be accelerated.

In addition to the circular source (actually a cylindrical source), square sources are also possible with the Fourier series solution. For this case, the source Fourier coefficients are

$$S_{mn} = \frac{S_{sq}}{2}\left[\frac{T_s}{T}\right]^2 \left[\frac{\sin\left(\alpha_n T_s / 2\right)}{\alpha_n T_s / 2}\right]\left[\frac{\sin\left(\alpha_m T_s / 2\right)}{\alpha_m T_s / 2}\right] \tag{15}$$

where T_s is the square source dimension.

One final application particularly lends itself to 2D benchmarks. Through superposition, individual sources can be added and subtracted to make relatively complex sources. Figures 4a,b show two of these. The first is a circular source embedded within the square source and the second is the square source embedded within the circular source. These configurations make challenging benchmarks indeed. It seems one could go on forever crafting sources within sources to develop particular transport configurations and more challenging benchmarks.

3.3. 2D Multigroup Homogeneous Medium

The 2D Multigroup benchmark follows along the same lines as the one-group benchmark, but in vector form. We assume a Watt fission spectrum for the energy source.

Finally, Fig. 5 gives the flux spectrum at the cell center for $G = 2^l$, l=2(1)8 groups specifically in the resonance region. The resonance structure becomes clearly defined as we include more groups.

CONCLUSION

In this presentation, we present only two of the 8 or so benchmarks that comprise the ATR benchmark suite. Each has been internally verified as well as crosschecked with the overlapping benchmarks within the suite. In a future effort, a corresponding suite is to be developed based on discrete ordinates and doubling.

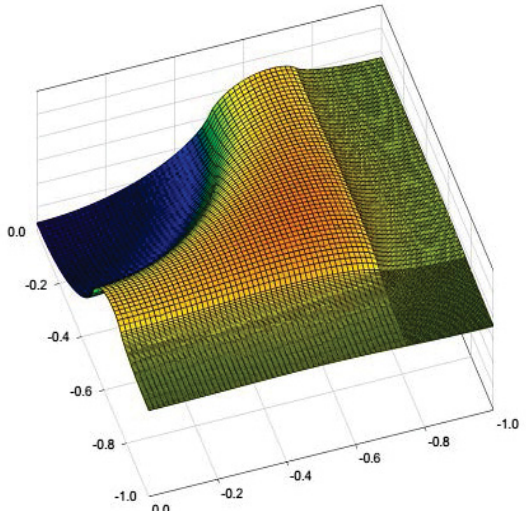

Fig. 4a. Flux for a circular source within a square source.

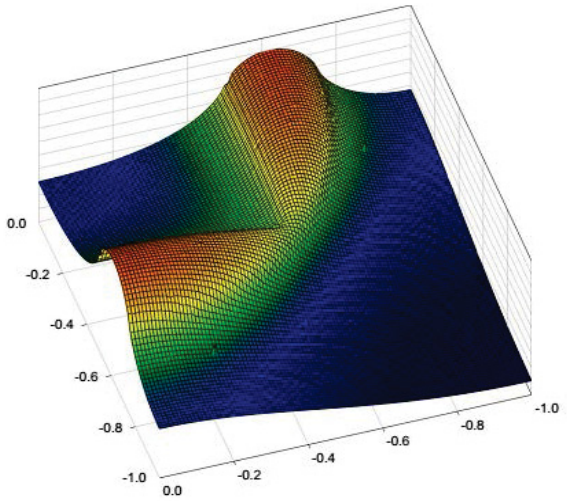

Fig. 4b. Flux for a square source within a circular source.

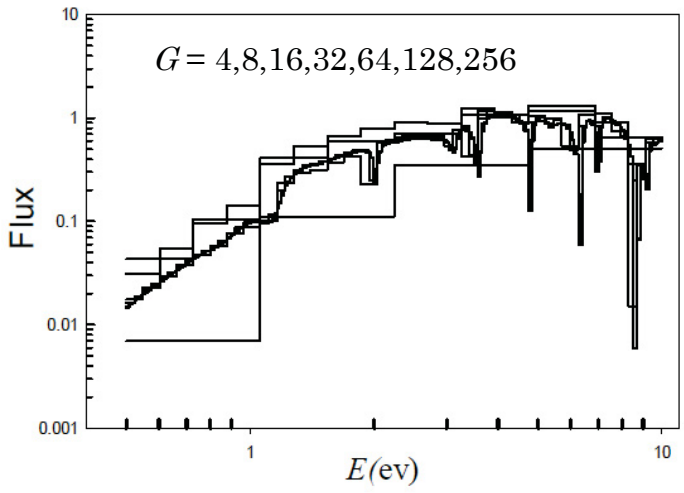

Fig. 5. Spectra cell center for resonance region.

REFERENCES

[1] D.W. NIGG AND K.A. STEUHM, Advanced Test Reactor Core Modeling Update Project: Annual Report for Fiscal Year 2011, INL/EXT-11-23348.

[2] MMR Williams, Exact Solutions of the Two-Dimensional Cell Problems, NSE: **173**, 182–196 2013.

[3] A. Sidi, *Practical Extrapolations Methods*, Cambridge University Press. Cambridge. 2003.

[4] http://www.nndc.bnl.gov/exfor/endf00.jsp